A Model of Spatial Reach in LFP Recordings

Henrik Lindén, Tom Tetzlaff, Szymon Łęski, Klas H. Pettersen, Sonja Grün, Markus Diesmann, and Gaute T. Einevoll

Abstract The measurement of local field potentials (LFP), the low-frequency part of extracellularly recorded potentials, is one of the most commonly used methods for probing hippocampal and cortical activity in vivo. It offers the possibility to monitor the activity of many neurons close to the recording electrode simultaneously but has the limitation that it may be difficult to interpret and relate to the underlying neuronal activity. The recording electrode picks up activity from proximal neurons, but what about more distant neurons? An important piece of information for a correct interpretation of the LFP is to decide the size of the tissue that substantially contributes to the LFP, i.e., the *reach* of the LFP signal. In this chapter we present a simple model that describes how population geometry, spatial decay of single-

H. Lindén (✉)
Department of Neuroscience, University of Copenhagen, Copenhagen, Denmark
e-mail: hlinden@sund.ku.dk

T. Tetzlaff
Institute of Neuroscience and Medicine (INM-6) and Institute for Advanced Simulation (IAS-6) and JARA Institute Brain Structure-Function Relationships (INM-10), Jülich Research Centre, Jülich, Germany
e-mail: t.tetzlaff@fz-juelich.de

S. Łęski
Department of Neurophysiology, Nencki Institute of Experimental Biology of Polish Academy of Sciences, Warsaw, Poland

K. H. Pettersen
Letten Centre and GliaLab, Department of Molecular Medicine, Institute of Basic Medical Sciences, University of Oslo, Oslo, Norway
e-mail: klas.pettersen@gmail.com

S. Grün
Institute of Neuroscience and Medicine (INM-6) and Institute for Advanced Simulation (IAS-6) and JARA Institute Brain Structure-Function Relationships (INM-10), Jülich Research Centre, Jülich, Germany

Theoretical Systems Neurobiology, RWTH Aachen University, Aachen, Germany
e-mail: s.gruen@fz-juelich.de

V. Cutsuridis et al. (eds.), *Hippocampal Microcircuits*, Springer Series in Computational Neuroscience, https://doi.org/10.1007/978-3-319-99103-0_13

cell LFP contributions, and correlation between LFP sources determine the relation between LFP amplitude and population size and use it to study the spatial reach of the LFP. The model can also be used to study different frequency bands of the LFP separately as well as the spatial decay outside the active neuronal population.

Overview

What is the Model

The recording of electrical potentials with extracellular electrodes has for many decades been the work horse in in vivo studies of cortical and hippocampal function (Buzsáki et al., 2012). The high-frequency part ($\gtrsim$500 Hz), the multiunit activity (MUA), mainly reflects spiking in neurons surrounding the electrode contact. In contrast, the low-frequency part, the local field potential (LFP), is thought to mainly reflect synaptic inputs and their subthreshold dendritic processing (Einevoll et al., 2013b) (at least for LFP frequencies below, say, 100 Hz Schomburg et al. 2012).

In the context of hippocampal studies, the LFP has commonly been used to investigate characteristic oscillations at a wide range of frequencies: low-frequency theta oscillations ($\sim$5–10 Hz) (Buzsáki, 2002), gamma oscillations ($\sim$30–100 Hz) (Bragin et al., 1995), and very high-frequency "ripples" ($\sim$100–200 Hz) (Ylinen et al., 1995; Siapas and Wilson, 1998; Maier et al., 2011). When recorded across the hippocampal lamina, the LFP has also been used to extract current source densities (CSDs) (Brankack et al., 1993; Sirota et al., 2003; Buzsáki et al., 2012) and to estimate synaptic pathways into the hippocampus (Herreras et al., 2015). Further, the hippocampal LFP has been shown to encode spatial position, in analogy with the spiking of hippocampal place cells (Agarwal et al., 2014; Taxidis et al., 2015).

The LFP is, despite its name, a much less local measure of neural activity than spikes as the signal in general stems from populations of thousands or more neurons surrounding the electrode (Einevoll et al., 2013a). Thus while offering

M. Diesmann
Institute of Neuroscience and Medicine (INM-6) and Institute for Advanced Simulation (IAS-6) and JARA Institute Brain Structure-Function Relationships (INM-10), Jülich Research Centre, Jülich, Germany

Department of Psychiatry, Psychotherapy and Psychosomatics, Medical Faculty, and Department of Physics, Faculty 1, RWTH Aachen University, Aachen, Germany
e-mail: m.diesmann@fz-juelich.de

G. T. Einevoll
Faculty of Science and Technology, Norwegian University of Life Sciences, Ås, Norway

Department of Physics, University of Oslo, Oslo, Norway
e-mail: gaute.einevoll@nmbu.no

an attractive opportunity for monitoring population activity, the LFP also has a strong limitation: it can be difficult to interpret where the signal comes from and what it represents. Proper mathematical modeling and analysis is thus needed to properly infer the underlying neural activity from the signal (Einevoll et al., 2013b). A key aspect for a correct interpretation of the LFP is knowing the size of the region that generates it, i.e., knowing the spatial reach of the LFP. A number of experimental studies have addressed this issue (Liu and Newsome, 2006; Kreiman et al., 2006; Berens et al., 2008; Katzner et al., 2009; Xing et al., 2009; Kajikawa and Schroeder, 2011) but have come with contradictory evidence regarding the spatial reach, ranging from a few hundred micrometers (Katzner et al., 2009; Xing et al., 2009) to several millimeters (Kreiman et al., 2006). One possible explanation for this discrepancy is that the reach of the LFP is not a fixed quantity, but rather changes with experimental conditions as the neuronal network state changes due to behavioral context, stimulation, or level of anesthesia.

For spikes, i.e., the extracellular signatures of action potentials extracted from the MUA, the definition of spatial reach is rather straightforward. Since (1) the spike amplitude decays sharply with distance between the neuron and the recording electrode and (2) spikes of relevant neighboring neurons typically are nonoverlapping in time, it is natural to ask at which distance a spike becomes indiscernible from the background noise (Buzsáki, 2004; Pettersen and Einevoll, 2008). For LFPs the situation is quite different. Since the LFP is primarily generated by slower synaptic events, the contributions from different sources are overlapping in time resulting in a signal that is a sum over many contributions.

So what determines the reach of the LFP? Intuitively, the reach of the LFP is the result of two opposing scaling effects: as in the case of extracellular action potentials, the contribution from a single neuron to the LFP still decays with distance from the recording electrode (Lindén et al., 2010), but the number of potentially contributing neurons increases with distance. There is, however, also a third important factor that influences the LFP: whether the LFP contributions from separate neurons are correlated or not. Just like water waves from several sources may interfere constructively if they are synchronized, both the amplitude as well as the spatial reach of the LFP may be drastically changed depending on the level of correlation in the generating neuronal population (Lindén et al., 2011).

Questions Addressed

In this chapter we describe a compact model of LFP generation that encapsulates how population geometry, single-cell features, and population-level correlations determine the size of the region generating the LFP measured in the center of a neuronal population (Einevoll et al., 2013b). The model can also be used to model the spatial decay outside the active neuronal population which, in turn, may help to understand the relative LFP contributions from simultaneously active neuronal populations.

The present model assumes passive dendrites and considers LFPs due to synaptic currents and the associated return currents but could straightforwardly be extended to model, e.g., active subthreshold conductances (Ness et al., 2015).

Levels of Detail/Rationale

The spatial reach of the LFP is difficult to measure experimentally because it is in general difficult to precisely control or measure the neuronal activity that generates the signal. To complicate matters further, the LFP can in principle be composed of contributions from several local and distant populations that spread via volume conduction. Here we take an analytical approach to address the question of LFP reach for a situation where a single population dominates the signal and derive a model that relies on numerical simulations of synaptically activated neurons for certain components of the model. This approach has the advantage that we can fully control both the size and activity of the neuronal population. Specifically, in contrast to experiments, we can vary the size of the population to study the effects on the LFP.

The Model

Model Components

Let us consider an LFP measured in the center of a disclike neuronal population (Fig. 1). The size of the population is defined by the radius R. Each cell i in the population gives a contribution $\phi_i(t)$ to the population LFP $\phi(t) = \sum_i \phi_i(t)$. How does the amplitude of the LFP fluctuations (that we here quantify by the standard deviation σ) increase with the population radius R? As we will explain below, the answer to this question depends on three factors:

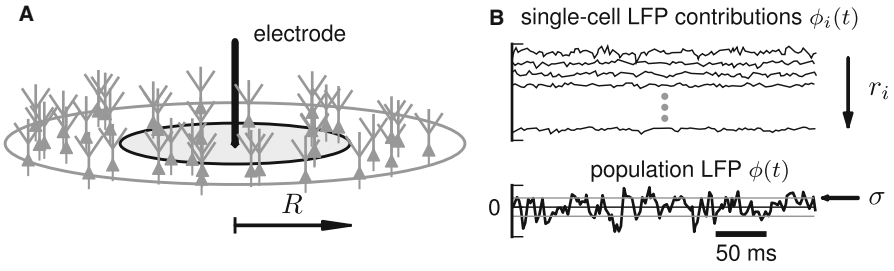

Fig. 1 Illustration of model setup. We study a model of the population LFP based on the spatial summation of single-neuron LFP contributions from many neurons. (**a**) An electrode is placed in the center of a disclike population, and by varying the radius R, we can investigate how the amplitude of the LFP increases with population radius. (**b**) Each neuron (ordered by their distance r_i from the recording electrode) gives a contribution $\phi_i(t)$ to the population LFP $\phi(t)$. The amplitude of the LFP is measured by the standard deviation σ of the LFP fluctuations over time. (Adapted with permission from Lindén et al. 2011)

1. The distance dependence of the amplitude of the single-neuron contributions $\phi_i(t)$ characterized by the shape function $F(r)$,
2. the number of neurons as a function of distance from the recording electrode, given by the population geometry,
3. the level of correlation between the LFP contributions from different neurons.

We will first turn to numerical simulations of single-cell LFP contributions generated by multi-compartment neuron models to find the shape functions $F(r)$ (point 1) and then derive an analytical expression for the LFP amplitude encapsulating all three factors above. Based on this we will give a precise definition of the reach of the LFP that we will test against full numerical population simulations and briefly describe how the model can be extended to study separate individual frequency components of the LFP (section "Results").

Single-Cell Shape Function

How does the amplitude of the LFP contribution from a cell depend on the distance to the recording electrode? To answer this question, we performed simulations of synaptically activated multi-compartment neuron models and computed the resulting LFP at the soma level for different radial distances to the electrode (Lindén et al., 2011). The LFP was calculated using the line-source formalism (Holt and Koch, 1999) as implemented in the software *LFPy* (http://lfpy.github.io) (Lindén et al., 2014), and the neurons were activated using uncorrelated spike trains. Results of these simulations are shown in Fig. 2.

We see that the amplitude typically decays as $\sim 1/r^2$ with distance r for distances further away than 200–300 μm from electrode (Fig. 2a, dashed line). This is consistent with the spatial decay of the electric potential generated by a current dipole. Closer to the electrode, the decay is less steep, roughly $\sim 1/r^{1/2}$. This is likely due to the dendritic extent of the neurons that typically is on the order of a few hundred micrometers.

This picture is very similar for neurons with different morphologies (Fig. 2a), but we see that the spatial decay changes somewhat for different synaptic input scenarios (Fig. 2b). The distance at which the decay changes slope from low to high is further away from the cell in the case of only apical input onto a pyramidal L5 neuron compared to when inputs are distributed basally or homogeneously over the whole cell. Because of the vertical extent of the pyramidal neuron (which is approximately 1200 μm), the synapses in this scenario are further away from the recording positions which also causes a lower amplitude of the LFP compared to basal input.

Based on these examples, we can formulate simplified expressions for the spatial decay $F(r)$ of the amplitude from a single-neuron LFP contribution (Einevoll et al., 2013a):

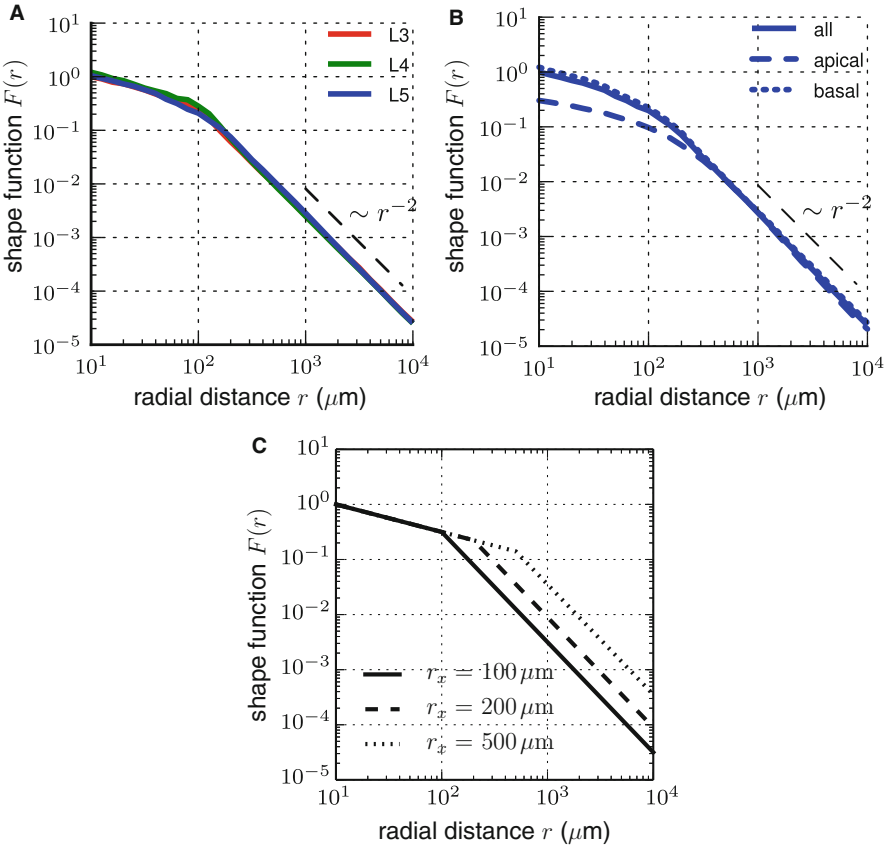

Fig. 2 Spatial decay of the LFP contribution from a single neuron. Multi-compartment neuron models were placed at different radial distances r away from a virtual recording electrode, and the LFP amplitude was computed at each distance. The distance dependence of the LFP amplitude is captured by the shape function $F(r)$ (see text). For further details of the simulation, we refer to Lindén et al. (2011). (**a**) Shape function for three types of cortical V1 neurons (layer 3 and layer 5 pyramidal neurons as well as a layer 4 stellate neuron). (**b**) Dependence of the shape function on the synaptic input region for the layer 5 pyramidal neuron. (**c**) Illustration of simplified shape function $F(r)$ given by Eq. 1 with $r_\epsilon = 10\,\mu$m and $F_0 = 1$ for three different values of the cutoff distance $r_x = [100,200,500]\,\mu$m (indicated by line style). ((**a**) and (**b**) adapted with permission from Lindén et al. 2011)

$$F(r) = \begin{cases} F_0 & r < r_\epsilon, \\ F_0 (r_\epsilon / r)^{1/2} & r_\epsilon < r \le r_x, \\ F_0 (r_\epsilon / r_x)^{1/2} (r_x / r)^2 & r \ge r_x, \end{cases} \tag{1}$$

where r_x is the *cutoff distance* where the decay changes slope and r_ϵ is a minimal radial distance introduced to avoid an unphysical divergence as r goes to zero. (This could represent, e.g., the distance to the cell closest to the electrode, but we leave this unspecified here.) For an illustration of this simplified shape function $F(r)$, see Fig. 2c.

Derivation of the Simplified Model

Let us now consider a population of neurons distributed in a disclike volume with radius R. How does the amplitude of compound LFP $\phi(t)$ measured in the center of the population depend on the population radius? In the following we will describe a simple analytical model that gives the answer to this question (Einevoll et al., 2013a).

First, let us assume that the contribution $\phi_i(t)$ from a neuron i can be decomposed into a temporal and spatial part:

$$\phi_i(t) = \xi_i(t)F(r_i) \tag{2}$$

where $\xi_i(t)$ is a time-dependent variable with zero mean and unit variance which describes the temporal fluctuations of the LFP contribution and $f(r_i)$ is the shape function described above.

For the disclike population considered here, the number of neurons at a specific distance r from the electrode is determined by:

$$N(r) = 2\pi r\rho \tag{3}$$

where ρ is the area density of neuronal LFP sources. If all LFP sources were *uncorrelated*, that is, $\mathrm{E}_t[\phi_i(t)\phi_j(t)] = 0$ for $i \neq j$ where $\mathrm{E}_t[\cdot]$ represents expectation value over time, the variance σ^2 of the LFP from cells at a particular distance would increase linearly with the number of LFP sources at that distance. In the continuum limit, the total LFP amplitude can be formulated as an integral (Lindén et al., 2011):

$$\sigma^2(R) = G_0(R) = \int_0^R dr\ N(r)F(r)^2 = \rho\int_0^R dr\ 2\pi r F(r)^2 \tag{4}$$

where we have made use of Eq. (3) above.

It is clear from this expression that the shape function $F(r)$ is the key factor determining the way the amplitude of the compound LFP increases with distance. In Fig. 3a, we show how the LFP amplitude $\sigma(R) = \sqrt{G_0(R)}$ increases with distance in the case of uncorrelated neuronal sources using the shape function defined in Eq. 1. We see from the plot that the LFP amplitude in this case quickly appears to saturate to a maximum value. It can be shown analytically (Lindén et al., 2011; Einevoll et al., 2013a) that when the spatial decay of neuronal sources decreases as $\sim 1/r^2$ or more steeply, the LFP amplitude indeed converges to a fixed values as $R \to \infty$. This convergence suggest an intuitive definition of the *reach of the LFP* as the population radius R^* at which the LFP amplitude $\sigma(R)$ has obtained a certain fraction α of the amplitude at infinite population size $\sigma(R \to \infty)$.

If, on the other hand, the LFP sources are completely *correlated*, i.e., $\mathrm{E}_t[\phi_i(t)\phi_j(t)] = E_t[\xi_i(t)\xi_j(t)]F_iF_j = F_iF_j$, the variance of the amplitude of

the compound LFP from cells at a particular distance increases as the square of the number of LFP sources at that distance, and we get (Lindén et al., 2011):

$$\sigma^2(R) = G_1(R) = \left(\int_0^R dr\ N(r)F(r)\right)^2 = \rho^2\left(\int_0^R dr\ 2\pi r F(r)\right)^2 \quad (5)$$

A more general expression valid for any level of correlation $c_\phi = \mathrm{E}_t[\phi_i(t)\phi_j(t)]$ between LFP sources is given by Lindén et al. (2011):

$$\sigma(R) = \sqrt{(1-c_\phi)G_0(R) + c_\phi G_1(R)}\,. \quad (6)$$

Here the terms for uncorrelated (Eq. 4) and correlated sources (Eq. 5) have been combined and are scaled by the correlation coefficient c_ϕ. Equation 6 can be computed by numerical integration of $G_0(R)$ and $G_1(R)$ for any shape function $F(r)$ and also for a numerically derived one as in Fig. 2. For the simplified shape function $F(r)$ given by Eq. 1, we may, however, even find analytical expressions for the results of the integrals in Eqs. 4 and 5 (Einevoll et al., 2013a):

$$G_0(R) = \begin{cases} F_0^2\rho\pi R^2 & R \le r_\epsilon, \\ F_0^2\rho\pi r_\epsilon(2R - r_\epsilon) & r_\epsilon \le R \le r_x, \\ F_0^2\rho\pi r_\epsilon(3r_x - r_\epsilon - r_x^3/R^2) & R \ge r_x, \end{cases} \quad (7)$$

$$G_1(R) = \begin{cases} F_0^2\rho^2\pi^2 R^4 & R \le r_\epsilon, \\ F_0^2\rho^2\frac{1}{9}\pi^2\left(r_\epsilon^2 - 4r_\epsilon^{1/2}R^{3/2}\right)^2 & r_\epsilon \le R \le r_x, \\ F_0^2\rho^2\frac{1}{9}\pi^2 r_\epsilon\left(r_\epsilon^{3/2} - (4 + 6\ln(R/r_x))r_x^{3/2}\right)^2 & R \ge r_x. \end{cases} \quad (8)$$

Frequency-Dependent Formulation of the Simplified Model

The simplified model outlined so far predicts the variance $\sigma^2 \sim \int df\ P(f)$ of the compound LFP, i.e., the integral of the LFP power spectrum $P(f)$. All frequency components are hence collapsed into a single measure. The model can however easily be reformulated to obtain a frequency-resolved version, resulting in the following expression for the power spectrum $P(f, R)$ of the compound LFP of a cell population of radius R, analogous to Eq. 6 (for details of the derivation, see Łęski et al. 2013):

$$P(f, R) = (1 - c_\phi(f))G_0(f, R) + c_\phi(f)G_1(f, R). \quad (9)$$

Here, $c_\phi(f)$ denotes the population-averaged coherence between single-cell LFP contributions. Analogous to Eqs. 4 and 5, the functions

$$G_0(f, R) = \int_0^R dr\ N(r)F(f, r)^2 \tag{10}$$

and

$$G_1(f, R) = \left(\int_0^R dr\ N(r)F(f, r) \right)^2 \tag{11}$$

are determined by the shape function $F(f, r)$ describing the dependence of the single-cell LFP amplitude at frequency f at the cell-electrode distance r and $N(r)$ giving the number of LFP sources at distance r (cf. Eq. 3 for a disclike population geometry). For the results shown in section "Frequency Dependence of LFP Power and Reach," we will use the phenomenological model of the shape function defined in Eq. 1. The frequency dependence of the shape function $F(f, r)$ results from introducing a frequency-dependent cutoff distance $r_x = r_x(f)$. This frequency dependence of the cutoff distance (Fig. 5a) is obtained by fitting $F(f, r)$ to the results of simulations of multi-compartment neurons stimulated by white-noise synaptic input, i.e., synaptic input with a flat power spectrum (same setup as explained in section "Single-Cell Shape Function"). The second source of frequency dependence in Eq. 9 is the LFP coherence $c_\phi(f)$. Again, the shape of $c_\phi(f)$ (Fig. 5b) is obtained from simulations of multi-compartment neurons fed by white, partially shared synaptic input (see section "Simulations with Multi-compartment Neuron Models").

Spatial Decay Outside the Neuronal Population

All the equations above apply to a scenario where the LFP electrode is placed in the center of the disclike population. The expressions for G_0 and G_1 can, however, also be extended to account for a situation where the electrode is placed at a distance X away from the center (Einevoll et al., 2013a):

$$\begin{aligned} G_0(R, X) &= \rho \int_{\{|\mathbf{r}| \le R\}} d^2r\ F(|\mathbf{r} - \mathbf{X}|)^2 \\ &= \rho \int_0^{2\pi} d\theta \int_0^R dr\ r\ F\left(\sqrt{(X - r\cos\theta)^2 + (r\sin\theta)^2}\right)^2, \end{aligned} \tag{12}$$

$$G_1(R, X) = \left(\rho \int\limits_{\{|\mathbf{r}| \le R\}} d^2r \; F(|\mathbf{r} - \mathbf{X}|)\right)^2$$
$$= \rho^2 \left(\int_0^{2\pi} d\theta \int_0^R dr \; r \; F\left(\sqrt{(X - r\cos\theta)^2 + (r\sin\theta)^2}\right)\right)^2. \quad (13)$$

Here, $\mathbf{r}$ denotes the position vectors of the LFP sources and $\mathbf{X}$ the vector $X\mathbf{e}_x$ with $\mathbf{e}_x$ being a unit vector in the x-direction.

Results

We will first go through some of the predictions of the simplified model derived above and then in the next section compare these predictions against numerical population simulations. Finally, we will briefly illustrate the spatial decay of the LFP outside the active population.

Analytical Predictions for Amplitude and Reach

The model equations above (Eqs. 4, 5 and 6) predict two qualitatively different scaling behaviors for uncorrelated and correlated neuronal activity, respectively. This is illustrated in Fig. 3a, b where the two components $\sqrt{G_0}$ and $\sqrt{G_1}$ are plotted separately for a population of radius 1 mm. In the case of uncorrelated activity, the amplitude $\sigma(R)$ of the compound LFP converges to a fixed value that would not increase even if the neuron population were infinitely sized (Fig. 3a, see also Lindén et al. 2011; Einevoll et al. 2013a). With the definition of spatial reach introduced above, as the population radius R^* where the LFP amplitude has obtained a fraction α of the infinite-size population, the LFP sources that are positioned within a radius R^* contributes a proportion α of the total LFP amplitude even if they are embedded in population with infinite size. In Lindén et al. (2011), and Einevoll et al. (2013a) we have used $\alpha = 0.95$ which is illustrated with a dashed line in Fig. 3a. In this case the spatial reach is small, roughly $\sim$200 μm.

In contrast, if the neuronal LFP sources were fully correlated, the amplitude increase with population radius is markedly different (Fig. 3b). In this case the LFP amplitude no longer converges to a fixed value. With the same definition of the spatial reach as in the uncorrelated case, the LFP now contains contributions from most of the neuronal population (>800 μm). Furthermore, the amplitude of the LFP is markedly higher.

For intermediate values of the correlation c_ϕ, the contributions from the two terms G_0 and G_1 are weighted according to Eq. 6 to give intermediate scaling behavior of the LFP amplitude compared to the uncorrelated or fully uncorrelated case

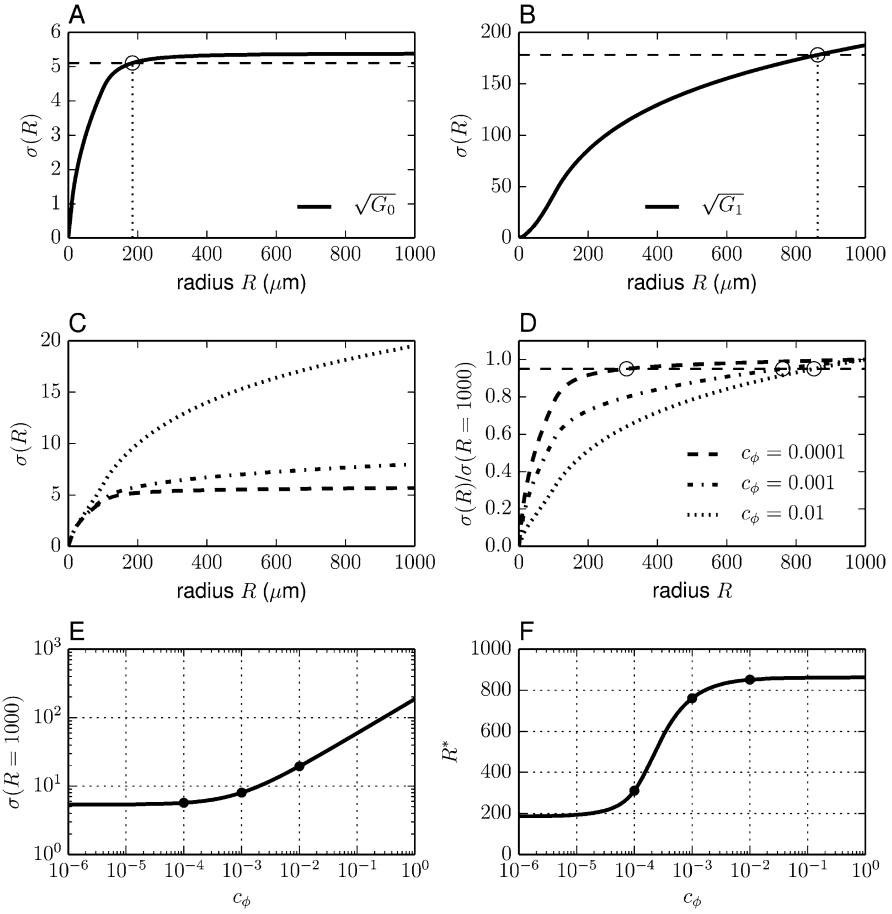

Fig. 3 Components of and results from the simplified model. Results of Eq. (6) using expressions for G_0 and G_1 given by Eqs.7 and 8 with area density $\rho = 10{,}000$ neurons/mm^2 derived using single-cell shape function $F(r)$ as defined in Eq. (1) with $r_\epsilon = 10\,\mu$m, $r_x = 100\,\mu$m and $F_0 = 1$. (**a**) When the LFP sources are uncorrelated, the amplitude $\sigma(R)$ of the compound signal is given by Eq. 4. In this case the amplitude converges to a fixed value for large R, and we here define the *spatial reach* of the LFP as the population radius R^* (dotted line) where the amplitude has obtained 95% of the maximum value (dashed line), here compared against the largest population radius considered in the study ($R = 1000\,\mu$m). (**b**) The amplitude $\sigma(R)$ in the case of fully *correlated* neuronal LFP sources, given by Eq. (5). (**c**) The LFP amplitude $\sigma(R)$ for intermediate levels of correlation c_ϕ (see legend in (**d**)). (**d**) Same as in (**c**), but normalized against the value at $R = 1000\,\mu$m. (**e**) LFP amplitude for population size $R = 1000\,\mu$m as a function of correlation level c_ϕ. (**f**) LFP reach R^* as a function of correlation level c_ϕ. Dots in (**e**) and (**f**) illustrate the examples shown in (**c**) and (**d**)

illustrated by three examples in Fig. 3c, d. As consequence, the LFP amplitude for large population radiuses becomes markedly higher as the correlation is increased (Fig. 3c). By normalizing the amplitude by that obtained for $R = 1000\,\mu$m, we show

in Fig. 3d how this affects the LFP reach: due to the larger increase in LFP amplitude with population radius, the spatial reach becomes larger with higher correlations.

In Fig. 3c, we plot the maximum LFP amplitude $\sigma(R = 1000\,\mu\text{m})$ for a wide range of correlations c_ϕ, and in Fig. 3d, the corresponding values for the LFP reach are shown. Already at low levels ($c_\phi =\sim 10^{-4}$), the correlations start to play a role in determining the LFP reach, and in the range between $\sim 10^{-4}$ and $\sim 10^{-2}$, there is a dramatic effect on the reach due to increasing correlation. Above this range ($\sim 10^{-2}$), the LFP is already getting substantial contributions from most of the population, and the reach does not increase further if the correlation level is increased. The amplitude $\sigma(R = 1000\,\mu\text{m})$, however, continues to increase up to the maximum correlation $c_\phi = 1$.

Simulations with Multi-compartment Neuron Models

The simplified LFP model described above neatly encapsulates the dependence of the LFP amplitude on the level of correlation between LFP contributions from different neurons in the population. In the above examples, we treated the level of correlation (c_ϕ) as a free parameter. In an experimental setting, however, the correlation between LFP sources depends on several factors, including (1) the correlation in synaptic input and (2) the spatial arrangement of dendrites and synaptic distributions on to the cells. As an example, one would expect larger LFP amplitude to be generated by synchronized input to spatially aligned cells with extended dendrites (in a so-called "open-field" arrangement) than asynchronous input on to spherically symmetric stellate cell (in so-called closed-field arrangements) (Mitzdorf, 1985; Lindén et al., 2010).

To test the predictions of the simplified model and to examine how the results depend on morphological features of the cells, we performed numerical simulations of populations of multi-compartment neuron models (Lindén et al., 2011) using digital reconstructions of V1 neurons from (Mainen and Sejnowski (1996)). We set up populations of 10,000 neurons in disclike populations of radius 1 mm (i.e., same scenario as in the model example above in Fig. 4) where correlations in the synaptic input could be systematically varied. This was done using a common pool of uncorrelated presynaptic spike trains with size N from which each neuron received n_{syn} spike trains. This generated a mean pair-wise correlation between the synaptic input to different cells of $c_\xi = n_{syn}/N$ (for details see Lindén et al. 2011). The resulting LFP was calculated using the line-source formalism (Holt and Koch, 1999; Lindén et al., 2014) for each cell separately, and the population LFP was then computed as a sum over contributions from cells within a specific radius R.

In Fig. 4a, b the results of such a simulation is shown for a population of pyramidal neurons activated by synapses distributed over the basal dendrites, for different levels of input correlation (indicated by line type). As predicted by the simplified model (Eq. 6), we see that the amplitude $\sigma(R)$ and the resulting LFP reach R^* are drastically changed by the correlation level. For this example, a change

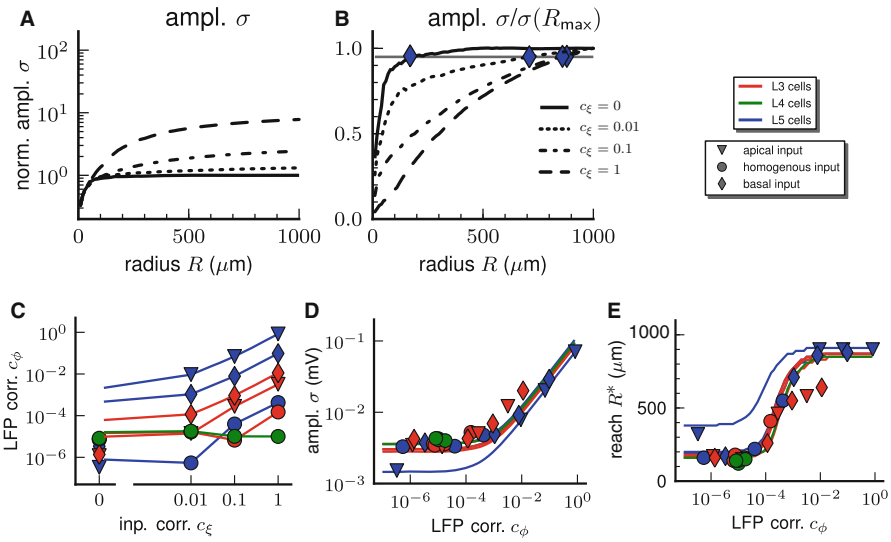

Fig. 4 Simulations of populations of multi-compartment neuron models. Results from the simplified model in Eq. 6 are compared with detailed numerical simulations of the LFP. Populations of 10,000 neurons were distributed in a disclike population with radius 1 mm^2 (layer 3 pyramidal neurons [red], layer 5 pyramidal neurons [blue], and layer 4 stellate neurons [green]). Neurons were synaptically activated using presynaptic spike trains from a common pool, and the degree of input correlation was varied by varying the pool size. The resulting LFP was computed using the line-source formalism (Holt and Koch, 1999). For details of the simulations we refer to Lindén et al. (2011). (**a**) LFP amplitude $\sigma(R)$ as a function of population radius R for a population of basally activated layer 5 pyramidal neurons. Line styles indicate the level of correlation between the incoming spike trains to different neurons (see inset in (**b**)). (**b**) Same as in (**a**), but normalized against the maximum value $\sigma(R = 1000\,\mu\text{m})$. (**c**) Resulting correlation c_ϕ between LFP contributions from different neurons in the population as a function of correlation c_ξ in incoming spike trains. Cell type and synaptic input region indicated by color and symbol (see inset). Lines show linear interpolation between numerical values (**d**) LFP amplitude $\sigma(R = 1000\,\mu\text{m})$ as a function of LFP correlation c_ϕ. (**e**) LFP reach R^* as a function of LFP correlation c_ϕ. In (**d**) and (**e**) lines show predictions from the simplified model (Eq. 6) using a numerically derived shape function $F(r)$ (as in Fig. 2) and symbols show numerical results for the LFP from population simulations. (Adapted with permission from Lindén et al. 2011)

between uncorrelation synaptic input $c_\xi = 0$ and fully correlated synaptic input $c_\xi = 1$ results in a change in spatial reach R^* of the LFP from small ($\sim$150 μm) to large ($\sim$800 μm) (Fig. 4b) accompanied by a tenfold increase in amplitude (Fig. 4a). For this example a correlation in synaptic input c_ξ in the range of [0,1] translates into a correlation between LFP contributions from different cells c_ϕ in the approximate range of $[10^{-6}, 10^{-1}]$ (Fig. 4c). According to the simplified model (Fig. 3f), this range covers the whole range of values in which the LFP reach is markedly affected by the correlations. For asymmetric input onto large extended dendrites like in this example, the simplified model thus correctly predicts that a change in correlation due to changing network state as a result of, e.g., external activation would increase

the spatial reach of the LFP from very local (for uncorrelated activity) to very large, essentially capturing the whole neuronal population (for correlated synaptic input to all neurons).

To test how general the above findings are, we also performed population simulations of other synaptic input regions (homogeneously distributed or only onto apical dendrites) and other cell types (smaller layer 3 pyramidal neurons and more symmetrical layer 4 stellate neurons) (Lindén et al., 2011). We found that the same range of synaptic correlations c_ξ resulted in very different ranges of LFP contribution correlations c_ϕ (Fig. 4c). For homogeneously distributed synaptic input onto asymmetric dendrites, the induced LFP correlations c_ϕ were smaller than for asymmetric input (to either basal or apical dendrites, see symbols in Fig. 4c), and for symmetric neurons, a change in the synaptic correlations did not substantially change the resulting LFP correlation (Fig. 4c, green). As a consequence, the same level of synaptic correlation will result in very different LFP amplitude $\sigma(R = 1000\,\mu\text{m})$ (Fig. 4d) and LFP reach (Fig. 4e) for different cell types and spatial distribution of synapses. The simplified model can notably capture this effect when the resulting LFP correlation is extracted from the numerical simulation and used with Eq. 6 (see lines in Fig. 4d, e). Note, however, that the model predictions differ slightly between simulations since we here used a shape function extracted from numerical simulations (as in Fig. 2) rather than a common simplified shape function given by Eq. 1.

Frequency Dependence of LFP Power and Reach

The investigation of LFPs is often focused on specific frequency bands. Research on hippocampal LFP, for example, often focuses on extracellular potentials in the theta band (~5–10 Hz; for a review, see Buzsáki 2002), gamma band (~30–100 Hz; e.g., Bragin et al. 1995), or even higher frequencies characteristic of "ripples" (~100–200 Hz; see Maier et al. 2011 and references therein), as well as interactions between these components (cross-frequency coupling; see, e.g., Belluscio et al. 2012). In the neocortex, the tuning properties (Liu and Newsome, 2006; Berens et al., 2008) and information contents (Belitski et al., 2008; Mazzoni et al., 2011) of the LFP are frequency-dependent. To understand the biophysical origin of LFP components at different frequencies and to correctly interpret experimental findings, it is essential to know which neuron populations contribute to the different frequency modes picked up at the recording electrode or, in other words, what the spatial reach of these different LFP components is. In Łęski et al. (2013), we approached this problem by means of a simplified mathematical model (see section "Frequency-Dependent Formulation of the Simplified Model") combined with simulations of multi-compartment neurons with realistic morphologies. Here, we will briefly summarize the main results of this study.

The simplified model outlined in section "Derivation of the Simplified Model" highlights three key factors dominating the power and reach of the compound LFP:

(1) the single-cell shape function $F(r)$, (2) the population geometry captured by the number of cells (LFP sources) $N(r)$ at distance r from the recording electrode, and (3) the coherence (correlation) c_ϕ between the LFP contributions of different cells. In general, the factors (1) and (3) depend on the frequency f, i.e., $F(r) = F(f, r)$ and $c_\phi = c_\phi(f)$.

We have previously observed (Pettersen and Einevoll, 2008; Lindén et al., 2010) that intrinsic dendritic filtering leads to low-pass filtering of the LFP. In effect, the single-cell shape functions are different for different frequency bands of the LFP. As shown in Łęski et al. (2013), this can be modeled by replacing the frequency-independent function $F(r)$ in Eq. (1) with its frequency-resolved counterpart $F(f, r)$, where the dependence on the frequency is fully captured by a frequency-dependent cutoff distance $r_x(f)$ (see Fig. 2c and section "Frequency-Dependent Formulation of the Simplified Model"). The decrease of $r_x(f)$ with frequency f (Fig. 5a) is observed across a range of different cell morphologies and synaptic input distributions (see Fig. 4 in Łęski et al. 2013). It can be understood as a reduction of the dendritic electrotonic length constant with increasing frequency: For higher frequencies, the transition to the dipole (far-field) decay $\sim r^{-2}$ occurs at smaller distances than for the low frequencies (Pettersen et al., 2012).

The frequency dependence of the shape function $F(f, r)$ alone is not sufficient to correctly predict the compound LFP power spectrum. The additional required ingredient is the frequency dependence of the coherence $c_\phi(f)$ between individual single-cell LFP contributions. The ultimate source of correlations between single-cell LFPs (i.e., nonvanishing $c_\phi(f)$) is correlated synaptic input which may result from the dynamics of the presynaptic networks and/or overlap in presynaptic cell populations (shared-input correlations). Input correlations arising from the network dynamics are typically frequency-dependent, i.e., $c_\xi = c_\xi(f)$. Network dynamics leading to oscillations, for example, often results in an increased synaptic input coherence at the oscillation frequency (Tetzlaff et al., 2008). Shared synaptic input, on the other hand, gives rise to frequency-independent input correlations c_ξ (Tetzlaff et al., 2008).

A priori, it is not obvious how correlations $c_\xi(f)$ between synaptic inputs are transferred to correlations $c_\phi(f)$ between single-cell LFP contributions at a particular frequency f. In general, this correlation transfer is modulated by dendritic filtering and by the variability in synapse positions and cell morphologies. Even if the synaptic input currents at all synapses of two different cells are identical ($c_\xi = 1$), differences in synapse positions and cell morphologies lead to nonidentical transmembrane current distributions and, hence, different LFP contributions ($c_\phi < 1$). Similar to the procedure described in section "Simulations with Multi-compartment Neuron Models," we measured the frequency dependence of the correlation transfer $c_\xi \mapsto c_\phi(f)$ in simulations of multi-compartment neurons receiving partially shared, white synaptic input (i.e., frequency-independent c_ξ).

For pyramidal neurons, we observe that the LFP coherence $c_\phi(f)$ is largest at low frequencies and decays monotonously with increasing frequency (see example in Fig. 5b). This observation can be explained by the fact that at higher frequencies, the return currents are closer to the synapse positions, so that the effective

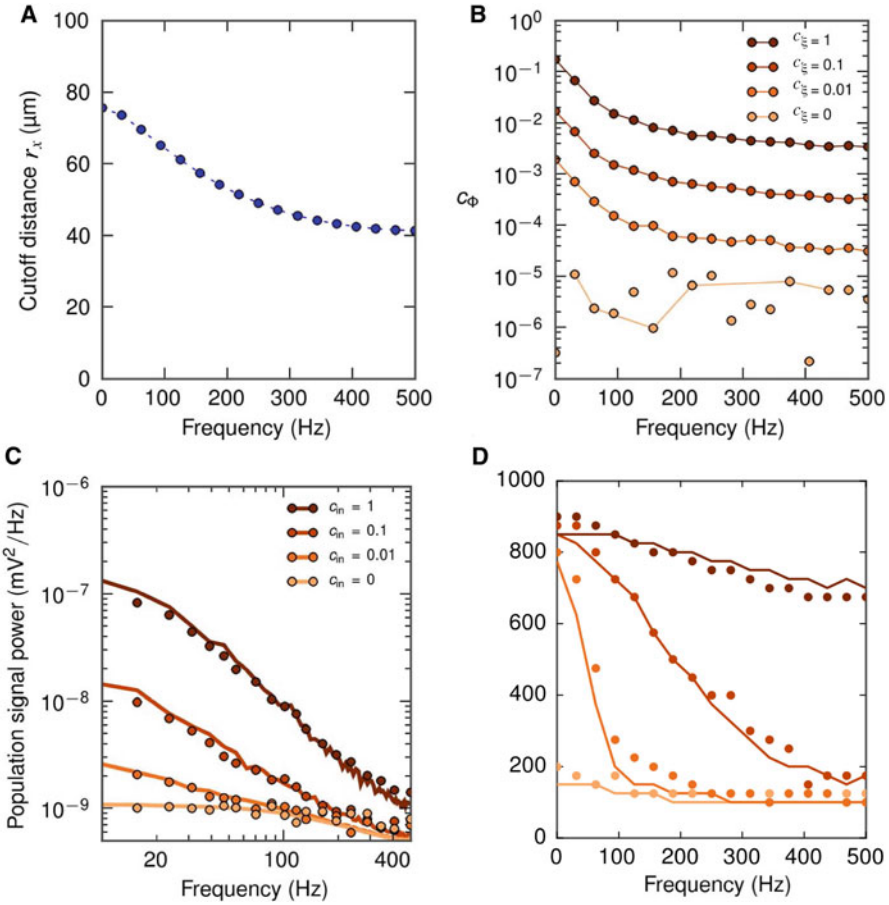

Fig. 5 Components and results of the frequency-resolved simplified model. (**a**) Frequency dependence of the cut-off distance r_x. (**b**) Frequency dependence of the population-averaged LFP coherence c_Φ for different input correlation levels c_ξ. (**c**) Power spectra of the total LFP in the center of a population of radius $R = 1000\,\mu$m. (**d**) Frequency dependence of the spatial reach. All panels show results for soma-level LFPs generated by cortical layer-5 pyramidal cells with white (frequency-independent) synaptic input to basal dendrites. Symbols in (**a**) and (**b**) depict results of multi-compartment-neuron simulations. Lines serve to guide the eye. Symbols not connected by lines indicate that the absolute value is plotted in place of spurious negative values. Lines and symbols in (**c**) and (**d**) show results of the simplified model (see section "Frequency-Dependent Formulation of the Simplified Model") and simulations for populations of multi-compartment neurons, respectively. (Adapted from Łęski et al. 2013)

current dipoles become shorter. For pyramidal neurons, the variability in dendrite orientation is largest at small spatial scales (e.g., within the basal bush). Hence, the high-frequency LFP components of individual neurons are decorrelated. At low frequencies, in contrast, the effective dipoles generated by synaptic input to pyramidal cells become larger and more aligned (parallel to the main cell axis).

For pyramidal cells, synaptic input correlations c_ξ are therefore more robustly transferred to LFP correlations c_ϕ at low frequencies than at high frequencies. For more symmetric stellate cells, the LFP correlations are typically much smaller (see Fig. 4c, green curve) and frequency-independent (Łęski et al., 2013).

Combining the frequency-dependent shape functions $F(f, r)$ and the LFP coherence $c_\phi(f)$ in the simplified model, Eq. (9) yields predictions for the power spectrum of the compound LFP (Fig. 5c) and the frequency dependence of the spatial reach (Fig. 5d). A comparison of the simplified-model predictions with the results of simulations of multi-compartment-neuron populations shows qualitative agreement for all investigated cell types and synapse distributions. In many cases, the predictions of the simplified model match the results of the simulations with multi-compartment models even quantitatively (compare dots and curves in Fig. 5c, d).

For pyramidal neurons, non-zero (frequency-independent) synaptic input correlations $c_\xi > 0$ can lead to a substantial amplification of the compound LFP power, in particular at low frequencies (Fig. 5c). The amplification of power at low frequencies results in a faster decay of the power spectrum. Note that this observation is compatible with findings showing larger EEG decay exponents during sleep as compared to awake states (Bédard et al., 2006). For vanishing input correlation $c_\xi = 0$, the frequency dependence of the reach is solely due to the frequency dependence of the cutoff distance $r_x(f)$. As a result, the frequency dependence of the reach is weak (Fig. 5d).

For nonvanishing input correlations $c_\xi > 0$, the compound LFP power and, hence, the LFP reach are more and more dominated by the frequency dependence of the LFP coherence $c_\phi(f)$. In the presence of intermediate input correlations $0 < c_\xi < 1$, the reach can exhibit a strong frequency dependence. For the example shown in Fig. 5d with $c_\xi = 0.01$, the reach can be as large as 800 μm at ∼0 Hz and drop to about 200 μm for frequencies above 100 Hz. For sufficiently large input correlations c_ξ, even the high-frequency LFP correlations c_ϕ become substantial (Fig. 5b). In consequence, the reach is close to the maximum population radius for all frequencies (cf. $c_\xi = 1$ in Fig. 5d).

Note that the results shown here were obtained for white synaptic input and frequency-independent (shared) input correlations c_ξ. In addition to the effects described here, the power and reach of the LFP at a particular frequency f are determined by the spectral properties of the synaptic input (e.g., resulting from the dynamics of presynaptic networks), in particular by the frequency dependence of $c_\xi(f)$. In general, our results suggest that the LFP power and reach are dominated by coherent frequency components. Due to the low-pass characteristics of the correlation transfer depicted in Fig. 5b, however, input components with non-zero coherence $c_\xi(f_1) = c^* > 0$ at some frequency f_1 will dominate components with the same level of coherence $c_\xi(f_2) = c^*$ at a higher frequency $f_2 > f_1$. Theta oscillations in the synaptic input, for example, would give rise to a larger LFP reach than gamma oscillations, even if the gamma coherence is as large as the coherence in the theta band.

Spatial Decay Outside the Neuronal Population

All the results shown so far have been for the situation where the LFP electrode is placed in the center of the neuronal population generating the LFP. Our simplified analytical formulas can, however, be extended to cover scenarios where the electrode is not in the center but some distance X away from the center position (see Eqs. 12 and 13). While we now return to the frequency-independent case and describe the total LFP amplitude σ as a sum over all frequencies, it should be noted that the spatial decay outside the population can in a similar manner as in Fig. 5 also be studied for different frequency components separately (for details and numerical results on this, we refer to Łęski et al. 2013).

In Fig. 6a we show how the LFP amplitude decays as a function of distance X for three different population sizes. For the case of *uncorrelated* LFP contributions, Eq. 6 gives that $\sigma(R, X) = \sqrt{G_0(R, X)}$ (solid lines), while the LFP from *completely correlated* LFP sources is given by $\sigma(R, X) = \sqrt{G_1(R, X)}$ (dotted lines).

For uncorrelated LFP sources, we see that there is a steep decay in LFP amplitude around the edge of the population. For all three population sizes plotted, the amplitude starts to decay around 200 μm from the edge of the population and has decreased to a fraction of ∼0.7 of the amplitude in the center of the population (Fig. 6a, solid lines) at the population boundary. When the electrode is moved away beyond the population boundary, the LFP amplitude decays quickly and has for all three population sizes decreased by a factor ten compared to the center amplitude within 250 μm from the population edge. Relative to the population radius, the spatial decay is however more steep for larger populations than for smaller ones, as seen in Fig. 6b.

For correlated LFP sources (Fig. 6a, b, dotted lines), the spatial falloff is less abrupt than for uncorrelated sources. In this case the LFP amplitude starts to decay considerably already for off-center positions close to the population center. Outside the population, the LFP extends further beyond the population edge than for uncorrelated activity (compared dotted and solid lines in Fig. 6a). This effect is more pronounced for larger populations than for smaller ones: while the amplitude decay for uncorrelated compared to correlated sources is very similar for a small population ($R = 250$ μm, Fig. 6a, black lines) outside the population, we see that the distance at which the amplitude has dropped to a fraction 0.1 of the center amplitude is increased for a population with radius $R = 1000$ μm to about 500 μm from the population boundary (Fig. 6a, green lines).

The simplified model formulated for off-center electrode positions (Eqs. 12 and 13) also allows us to examine how much crosstalk one would expect between neighboring populations, i.e., to which extent the LFP recorded in the center of one population would also contain contributions (or noise) from other neighboring neuronal populations. In Fig. 6c we show an example of such a situation with two neighboring populations with radius $R = 250$ μm that are positioned right next to each other. We assume that the two populations are uncorrelated with each other and

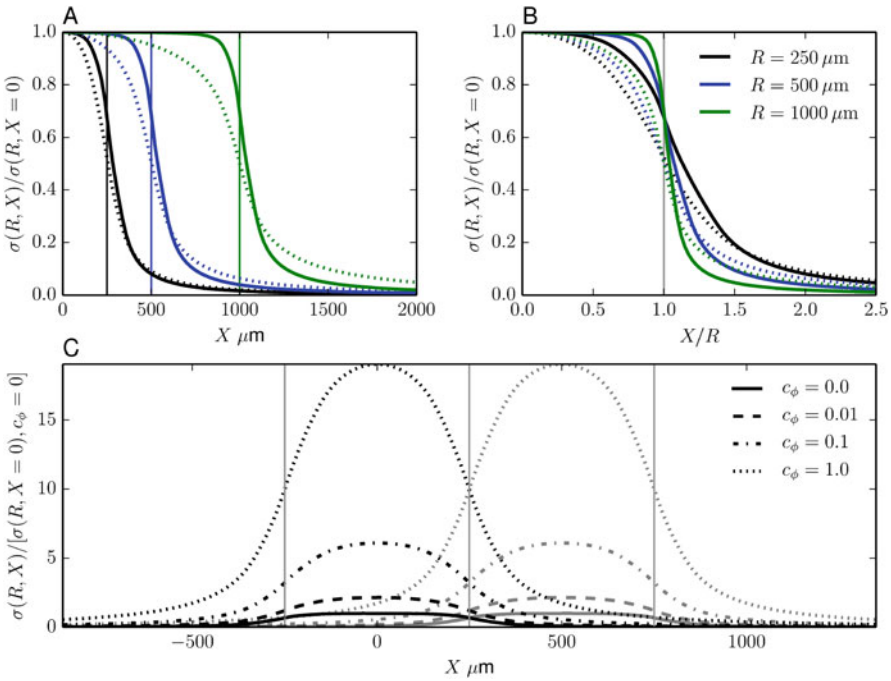

Fig. 6 Predictions for spatial decay outside the neuronal population. LFP amplitude $\sigma(R, X)$ at a distance X from the center of a population with radius R calculated from Eq. 6 using numerical integration of Eqs.12 and 13 with single-cell shape function $F(r)$ as defined in Eq. 1 for parameters $\rho = 10{,}000$ neurons/mm^2, $r_\epsilon = 10\,\mu$m, $r_x = 100\,\mu$m and $F_0 = 1$. (**a**) LFP amplitude $\sigma(R, X)$ for three different population sizes $R = [250{,}500{,}1000]\,\mu$m (indicated by color) for uncorrelated (solid lines) and correlated (dotted lines) LFP contributions. Curves have been normalized to the amplitude at the center of the population $\sigma(R, X = 0)$. (**b**) Same as in A with x-axis normalized by the population size R. (**c**) LFP amplitudes for two neighboring populations with radius $R = 250\,\mu$m centered at $X = 0$ and $X = 500\,\mu$m, respectively, for different levels of correlation c_ϕ (indicated by line style). Curves have been normalized to the LFP amplitude in the center of the population for uncorrelated LFP sources ($c_\phi = 0$). In all plots thin vertical lines represent the edge of the population

plot the LFP from each population separately. We see that the level of correlation between LFP sources in one population has a large effect on the overall amplitude of the LFP from that population as we would expect from our previous results on the LFP in the center of the population (see, e.g., Eq. 6 and Fig. 3e). This, however, also means that if the LFP sources within one population have a high degree of correlation, there is a large "spillover" to the neighboring population. In the example in Fig. 6c, we note that if we have one LFP electrode in the center of each population, the LFP generated by the *other* population may actually be larger than that from the local population, if the neighboring population is correlated, while the local population is uncorrelated. This, however, assumes that the overall activity in both populations is the same and that nothing else differs than the level of correlation

between LFP contributions within the populations. Since the overall LFP amplitude depends on several factors, such as synaptic strengths and activation rates, as well as synaptic placement (Lindén et al., 2011), a proper assessment of crosstalk would require a more detailed analysis. This is beyond the scope of this chapter, however.

Model Justification

Data for Model Components and Parameter Values

The simplified LFP model presented in this chapter is valid for a range of parameter values which are explicitly stated in the model formulation and does therefore not rely on specific choices of parameters. The model formulation was, however, made using a number of assumptions which we will list and discuss below.

Population geometry The presented formulation of the simplified model assumes a cylinder-like population geometry which seems like a good first approximation for several brain regions with a prominent layer structure as found both in the hippocampus and cortex. If the spatial reach is large enough, as the model predicts for a large area with correlated LFP sources, this assumed population geometry may be oversimplified. In the dentate gyrus, for example, the macroscopic curvature of the brain tissue creates large LFPs that are even larger *outside* the synaptically activated region that generates it (Fernandez-Ruiz et al., 2013). To model such brain regions, one would have to extend the model using a more realistic geometry (see below).

Spatially homogeneous LFP correlations When deriving the simplified model, we assumed that the LFP contribution from each cell can be decomposed into a temporal and spatial part (Eq. 2). As a consequence, the correlation between the LFP contributions from cells will be independent of the distance to the recording electrode, and we could therefore use a single parameter c_ϕ to represent the correlation for the entire population. Due to spatially distributed synapses and dendritic filtering (Lindén et al., 2011), we expect this assumption to not be valid under all circumstances. Indeed, when comparing with detailed population simulations, we saw some deviations that may be due to this assumption (see red markers in Fig. 4e). In the frequency-dependent model formulation (Eqs. 9, 10 and 11), we correspondingly assume the coherence to be spatially homogenous. While the model could be extended to include distant-dependent measures of correlation/coherence (see below), the simplified model performs quite well in comparison with the detailed numerical simulations also in the present form.

Definition of cells as individual LFP sources The model presented in this chapter views each cell as an individual LFP source, and the shape function $F(r)$ consequently describes the spatial decay of single-cell LFP contributions (Fig. 2). It would, however, be equally possible to formulate the model at the level of synapses,

so that the total LFP would be a sum over synaptic contributions, where different classes of synapses (based on, e.g., their spatial positioning on the dendrites) could be assigned different shape functions.

LFP calculations The LFP calculations in the detailed simulations were made assuming a linear, isotropic, homogenous, and ohmic extracellular medium which seems to be well-fulfilled for the frequencies studied here (Nunez and Srinivasan, 2006; Logothetis et al., 2007) (for further discussion, see Pettersen et al. 2012.) If warranted, however, other assumption about the extracellular medium could be accounted for in the biophysical forward-modeling scheme (Lindén et al., 2014) used to compute the shape function $F(r)$ and the LFP population correlation coefficient c_ϕ.

Passive dendritic conductances The present model assumes passive (RC) dendrites, but it can be extended to include active dendritic conductances. In particular, a recent study showed that the effect of subthreshold active conductances on the single-neuron LFP contribution, and thus the shape function $F(r)$, can be well described by means of so-called "quasi-active" linearization (Ness et al., 2015). Thus these active conductances can be included in the model without introducing any nonlinearity in the LFP generation, thus still allowing each frequency component to be treated independently in the model.

Successes and Limitations

The simplified model presented in this chapter encapsulates how the amplitude and reach of the LFP depends on three crucial factors: (1) the population geometry, (2) the spatial decay of single-neuron LFP contributions, and (3) the correlation between the LFP contributions from different cells. As the level of correlation between LFP sources depends on the state of the underlying network dynamic, our model demonstrates that the reach of the LFP is not a fixed quantity, but changes with the network state. Our model, thus, offers a putative explanation to the disparity between different experimental studies investigating the LFP reach, with estimates ranging from a few hundred micrometers (Katzner et al., 2009; Xing et al., 2009) to several millimeters (Kreiman et al., 2006).

The simplified model can straightforwardly be formulated in a frequency-specific manner that allows the investigation of different frequency bands of the LFP separately. The limited results shown here illustrate how frequency-specific spatial decay of single-cell contributions combined with frequency-specific coherence between LFP sources may lead to substantially larger spatial reach for low-frequency components of the LFP compared to higher frequencies. This directly influences the power spectrum of the LFP to have higher power at low compared to high frequencies.

The above results have focused on situations with the electrode placed in the center of the population at the depth of the somata, but the simplified model has proven equally applicable for other electrode positions; for example, see Lindén et al. (2011), and Łęski et al. (2013).

The Future

Model Extensions

The model presented in this chapter could be extended in several ways. As mentioned above a natural extension would be to adapt it for more realistic population geometries. This would be of particular interest for brain regions that have a clear macroscopic structure as, for instance, in the dentate gyrus. It has been shown by combined experimental and modeling work that for this particular system the curved shape of the cellular layers creates large amplitude LFPs that are due to the spatial summation of LFP contributions from different sites at the curved structure (Fernandez-Ruiz et al., 2013). To extend the model presented here to study such effects, one would have to replace Eq. 3 with a more appropriate expression and perform the analytical model derivation based on that. Alternatively, a numerical integration of Eqs. 4 and 5 using appropriate summation boundaries can also be done.

For some experimental setups, it may also be relevant to relax the assumption of homogeneous LFP correlations (see above) to include finer spatial structure of correlations. This could be important for capturing LFP correlations induced by spatially specific external inputs or for specific connectivity structures of the underlying neuronal circuits. This would make the integral expressions in Eqs. 4 and 5 more complicated; one can always use numerical summation of LFP sources to compute estimates of the spatial reach of the LFP.

New Uses of Model

The model presented in this chapter does not make any assumptions about the underlying neuronal network activity. In the multi-compartment simulations, we used random (Poissonian) spike trains to activate synapses and a simple common-input model to generate correlations between the input to different cells. Since LFP computed from the multi-compartment models with current-based synapses are linear with respect to the input level (see Lindén et al. 2011; Łęski et al. 2013), only the mean input correlation will affect the resulting LFP reach, while the synaptic rate will only affect the resulting LFP amplitude (through the constant F_0 in Eq. 1).

To use our model for a specific experimental setup, it would be possible to adapt our model to more closely match the hippocampal (or cortical) region of study. This could be done through the following steps:

1. By extracting the single-cell shape function $F(r)$ using reconstructed morphologies from the specific hippocampal (or cortical) area under study using a similar approach as in Fig. 2.
2. To use a more realistic model of spiking dynamics that would give a correlation structure in the synaptic inputs with, e.g., realistic oscillatory dynamics in frequency bands of interest. If these inputs then were used to activate multicompartment neuron models (similar to the setup illustrated in Fig. 4), the transfer from correlation between input spikes to correlation between LFP contributions could be estimated (as in Fig. 4c).
3. By setting the upper limit of population radius R according to known geometrical constraints in the region of study.

This could allow a detailed investigation of the LFP amplitude and the LFP reach for, e.g., theta compared to gamma oscillations.

Acknowledgements This work was done with financial support from the Danish Council for Independent Research and FP7 Marie Curie Actions – COFUND (grant id: DFF – 1330-00226), the European Union Seventh Framework Programme (FP7/2007-2013) under grant agreement 604102 (Human Brain Project, HBP) and grant agreement 269912 (BrainScaleS), the Helmholtz Association through the Helmholtz Portfolio Theme "Supercomputing and Modeling for the Human Brain" (SMHB), Jülich Aachen Research Alliance (JARA), and the Research Council of Norway (NFR, through ISP, NOTUR -NN4661K).

References

Agarwal G, Stevenson IH, Berényi A, Mizuseki K, Buzsáki G, Sommer FT (2014) Spatially distributed local fields in the hippocampus encode rat position. Science 344(6184):626–630

Bédard C, Kröger H, Destexhe A (2006) Does the $1/f$ frequency scaling of brain signals reflect self-organized critical states? Phys Rev Lett 97:118102

Belitski A, Gretton A, Magri C, Murayama Y, Montemurro MA, Logothetis NK, Panzeri S (2008) Low-frequency local field potentials and spikes in primary visual cortex convey independent visual information. J Neurosci 28(22):5696–5709

Belluscio MA, Mizuseki K, Schmidt R, Kempter R, Buzsáki G (2012) Cross-frequency phase-phase coupling between theta and gamma oscillations in the hippocampus. J Neurosci 32(2):423–435

Berens P, Keliris GA, Ecker AS, Logothetis NK, Tolias AS (2008) Comparing the feature selectivity of the gamma-band of the local field potential and the underlying spiking activity in primate visual cortex. Front Syst Neurosci 2:2

Bragin A, Jando G, Nadasdy Z, Hetke J, Wise K, Buzsáki G (1995) Gamma (40–100 Hz) oscillation in the hippocampus of the behaving rat. J Neurosci 15(1):47–60

Brankack J, Stewart M, Fox SE (1993) Current source density analysis of the hippocampal theta rhythm: associated sustained potentials and candidate synaptic generators. Brain Res 615: 310–327

Buzsáki G (2002) Theta oscillations in the hippocampus. Neuron 33(3):325–340

Buzsáki G (2004) Large-scale recording of neuronal ensembles. Nat Neurosci 7(5):446–451
Buzsáki G, Anastassiou C, Koch C (2012) The origin of extracellular fields and currents–EEG, ECoG, LFP and spikes. Nat Rev Neurosci 13:407–420
Einevoll GT, Lindén H, Tetzlaff T, Łęski S, Pettersen KH (2013a) Local field potentials: biophysical origin and analysis. In: Quiroga QR, Panzeri S (eds) Principles of neural coding. Taylor & Francis, CRC Press, Boca Raton
Einevoll GT, Kayser C, Logothetis N, Panzeri, S (2013b) Modelling and analysis of local field potentials for studying the function of cortical circuits. Nat Rev Neurosci 14:770–785
Fernandez-Ruiz A, Muñoz S, Sancho M, Makarova J, Makarov VA, Herreras O (2013) Cytoarchitectonic and dynamic origins of giant positive local field potentials in the dentate gyrus. J Neurosci 33(39):15518–15532
Herreras O, Makarova J, Makarov VA (2015) New uses of LFPs: pathway-specific threads obtained through spatial discrimination. Neuroscience 310:486–503
Holt GR, Koch C (1999) Electrical interactions via the extracellular potential near cell bodies. J Comp Neurol 6(2):169–184
Kajikawa Y, Schroeder CE (2011) How local is the local field potential? Neuron 72:847–858
Katzner S, Nauhaus I, Benucci A, Bonin V, Ringach DL, Carandini M (2009) Local origin of field potentials in visual cortex. Neuron 61:35–41
Kreiman G, Hung CP, Kraskov A, Quiroga RQ, Poggio T, DiCarlo JJ (2006). Object selectivity of local field potentials and spikes in the macaque inferior temporal cortex. Neuron 49:433–445
Łęski S, Lindén H, Pettersen KH, Einevoll GT (2013) Frequency dependence of signal power and spatial reach of the local field potential. PLoS Comput Biol 9(7):e1003137
Lindén H, Pettersen KH, Einevoll GT (2010). Intrinsic dendritic filtering gives low-pass power spectra of local field potentials. J Comp Neurol 29(3):423–444
Lindén H, Tetzlaff T, Potjans TC, Pettersen KH, Grün S, Diesmann M, Einevoll GT (2011) Modeling the spatial reach of the LFP. Neuron 72:859–872
Lindén H, Hagen E, Łęski S, Norheim ES, Pettersen KH, Einevoll GT (2014) LFPy: a tool for biophysical simulation of extracellular potentials generated by detailed model neurons. Front Neuroinform 7:41
Liu J, Newsome WT (2006) Local field potential in cortical area MT: stimulus tuning and behavioral correlations. J Neurosci 26(30):7779–7790
Logothetis NK, Kayser C, Oeltermann A (2007) In vivo measurement of cortical impedance spectrum in monkeys: implications for signal propagation. Neuron 55:809–823
Maier N, Tejero-Cantero A, Dorrn AL, Winterer J, Beed PS, Morris G, Kempter R, Poulet JF, Leibold C, Schmitz D (2011) Coherent phasic excitation during hippocampal ripples. Neuron 72:137–152
Mainen ZF, Sejnowski TJ (1996) Influence of dendritic structure on firing pattern in model neocortical neurons. Nature 382(6589):363–366
Mazzoni A, Brunel N, Cavallari S, Logothetis NK, Panzeri S (2011) Cortical dynamics during naturalistic sensory stimulations: experiments and models. J Physiol Paris 105(1–3):2–15
Mitzdorf U (1985) Current source-density method and application in cat cerebral cortex: investigation of evoked potentials and EEG phenomena. Physiol Rev 65(1):37–100
Ness TV, Remme MWH, Einevoll GT (2015) Active subthreshold dendritic conductances shape the local field potential. arXiv 1512.04293
Nunez PL, Srinivasan R (2006) Electric fields of the brain, 2nd edn. Oxford University Press, Inc., New York
Pettersen KH, Einevoll GT (2008) Amplitude variability and extracellular low-pass filtering of neuronal spikes. Biophys J 94(3):784–802
Pettersen KH, Lindén H, Dale AM, Einevoll GT (2012) Extracellular spikes and current-source density. In Brette R, Destexhe A (eds) Handbook of neural activity measurement. Cambridge University Press, Cambridge
Schomburg EW, Anastassiou CA, Buzsáki G, Koch C (2012) The spiking component of oscillatory extracellular potentials in the rat hippocampus. J Neurosci 32:11798–11811

Siapas AG, Wilson MA (1998) Coordinated interactions between hippocampal ripples and cortical spindles during slow-wave sleep. Neuron 21:1123–1112

Sirota A, Csicsvari J, Buhl D, Buzsáki G (2003) Communication between neocortex and hippocampus during sleep in rodents. Proc Natl Acad Sci USA 100:2065–2069

Taxidis J, Anastassiou CA, Diba K, Koch C (2015) Local field potentials encode place cell ensemble activation during hippocampal sharp wave ripples. Neuron 87(3):590–604

Tetzlaff T, Rotter S, Stark E, Abeles M, Aertsen A, Diesmann M (2008) Dependence of neuronal correlations on filter characteristics and marginal spike-train statistics. Neural Comput 20(9):2133–2184

Xing D, Yeh C-I, Shapley RM (2009) Spatial spread of the local field potential and its laminar variation in visual cortex. J Neurosci 29:11540–11549

Ylinen A, Bragin A, Nádasdy Z, Jandó G, Szabó I, Sik A, Buzsáki G (1995) Sharp wave-associated high-frequency oscillation (200 Hz) in the intact hippocampus: network and intracellular mechanisms. J Neurosci 15:30–46